Resistivity Tensor of Vortex-Lattice States in Josephson Junction Arrays

Alexander-Georg Penner[®], ¹ Karsten Flensberg, ² Leonid I. Glazman, ³ and Felix von Oppen[®] ¹Dahlem Center for Complex Quantum Systems and Fachbereich Physik, Freie Universität Berlin, 14195 Berlin, Germany

²Center for Quantum Devices, Niels Bohr Institute, University of Copenhagen, DK-2100 Copenhagen, Denmark ³Department of Physics, Yale University, New Haven, Connecticut 06520, USA

(Received 1 July 2023; accepted 17 October 2023; published 14 November 2023)

Two-dimensional Josephson junction arrays frustrated by a perpendicular magnetic field are predicted to form a cascade of distinct vortex lattice states. Here, we show that the resistivity tensor provides both structural and dynamical information on the vortex-lattice states and intervening phase transitions, which allows for experimental identification of these symmetry-breaking ground states. We illustrate our general approach by a microscopic theory of the resistivity tensor for a range of magnetic fields exhibiting a rich set of vortex lattices as well as transitions to liquid-crystalline vortex states.

DOI: 10.1103/PhysRevLett.131.206001

Introduction.—Josephson junction arrays display a fascinating variety of classical and quantum phases [1,2]. In the absence of charging effects, the system undergoes a temperature-driven Berezinskii-Kosterlitz-Thouless transition between a superconducting and a resistive phase. When the charging energy becomes large, quantum fluctuations destroy coherence between the superconducting islands already at zero temperature, inducing a superconductor-insulator transition. Particularly rich phase structure appears in a perpendicular magnetic field, even in the classical limit [3–6]. The magnetic field results in a cascade of vortex-lattice ground states, which spontaneously break the lattice symmetry of the array [7,8]. While their equilibrium properties have been widely studied numerically [7–16], experimental studies have been lagging in identifying and probing these vortex-lattice states and little is known theoretically about their transport properties [17,18].

Here, we show that the resistivity tensor is a powerful tool to probe these vortex-lattice phases. Measurements of the longitudinal and transverse resistivity of Josephson junction arrays reveal a dramatic sensitivity to the perpendicular magnetic field [4,19,20]. This dependence reflects the sensitive dependence of the ground state on the ratio f of the magnetic flux ϕ per plaquette and the superconducting flux quantum $\phi_0 = h/2e$. Our principal observations are twofold. First, the spontaneous breaking of the lattice symmetry generally makes the resistivity tensor anisotropic, with the anisotropy encoding structural information on the vortex lattice. Second, phase transitions from vortex lattices to liquid-crystalline states [13,21] are signaled by the temperature dependence of the resistivity tensor. Importantly, full information is revealed only when measuring the entire resistivity tensor, which has not yet been done in experiments.

Our work is motivated by recent advances in nanofabricating Josephson junction arrays using semiconductor-superconductor hybrids [22]. These arrays are exceptionally flexible in their lattice geometry and have outstanding tunability of the junction properties [23–25]. Work to date has focused on the Berezinskii-Kosterlitz-Thouless transition [23,24] and vortex dynamics [25]. This generation of devices should readily admit measurements of the entire resistivity tensor, significantly advancing the experimental study of vortex lattices in Josephson junction arrays.

Model.—We describe the superconducting islands of the array as classical xy spins. Neighboring spins are subject to an effective ferromagnetic interaction due to the Josephson coupling of strength E_J between islands and the perpendicular magnetic field introduces frustration into the xy model,

$$H = -E_J \sum_{\langle ij \rangle} \cos(\varphi_i - \varphi_j + 2\pi a A_{ij}/\phi_0). \tag{1}$$

We note that we neglect self-inductance effects [26–30], which can be estimated to be weak for the arrays studied in Refs. [23–25]. We also assume that charging energies can be neglected, so that finding the equilibrium state of the array (lattice constant a) is a problem of classical statistical mechanics. The magnetic field is accounted for by the vector potential A_{ij} , with the flux

$$\phi = f\phi_0 = \sum_{\text{plaquette}} aA_{ij},\tag{2}$$

per plaquette in units of the superconducting flux quantum $\phi_0 = h/2e$ defining the frustration f. Without magnetic field, it is energetically favorable for the phases φ_i of all superconducting islands to align.

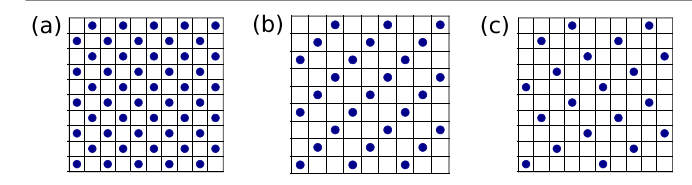


FIG. 1. Vortex-lattice ground states for frustrations (a) f = 1/2, (b) f = 1/3, and (c) f = 1/5.

A magnetic field introduces vortices, which have a natural inclination to order. The vortex lattice is a sensitive function of the magnetic field, reflecting the competition between the intrinsic tendency of vortices to order into a triangular structure and pinning by the lattice (which we take to be a square array). This is exemplified in Fig. 1 for simple rational frustrations. For f=1/2, the vortices form a checkerboard, breaking the discrete translation symmetry of the array, but leaving its C_4 rotation symmetry intact [Fig. 1(a)]. For f=1/3, the vortices occupy plaquettes along every third diagonal, which also breaks the rotation symmetry down to C_2 [Fig. 1(b)]. At other frustrations such as f=1/5, the principal axes of the vortex lattice do not align along the diagonals of the square array [Fig. 1(c)].

Resistivity tensor.—For a square junction array, the resistivity is isotropic as long as the ground state respects the underlying fourfold symmetry, e.g., at $f = \frac{1}{2}$. More generally, however, the formation of a symmetry-breaking vortex lattice will be signaled by an anisotropic resistivity tensor. The resistivity tensor is a sum of symmetric and antisymmetric contributions,

$$\rho = \begin{pmatrix} \rho_{xx} & \rho_{xy}^s \\ \rho_{xy}^s & \rho_{yy} \end{pmatrix} + \begin{pmatrix} 0 & \rho_H \\ -\rho_H & 0 \end{pmatrix}. \tag{3}$$

The symmetric contribution describes the dissipative resistivity with eigenvalues ρ_1 and ρ_2 . The antisymmetric contribution is invariant under changes of the coordinate system and describes the Hall resistivity ρ_H . Because of the Onsager relation $\rho_{xy}(B) = \rho_{yx}(-B)$, the two contributions ρ_{xy}^s and ρ_H to the transverse resistance ρ_{xy} can be separated by their behavior under reversal of the perpendicular magnetic field B. While the Hall resistivity ρ_H is odd under reversal of the magnetic field, $\rho_H(B) = -\rho_H(-B)$, the transverse resistivity ρ_{xy}^s is even, $\rho_{xy}^s(B) = \rho_{xy}^s(-B)$. This is in line with the fact that the eigenvalues ρ_j (with j=1,2) are even in B.

It follows from this discussion that measurements of the full resistivity tensor reveal rich information on the vortexlattice states. The eigenvalues ρ_1 and ρ_2 encode the density of mobile vortices and their mobility, while the principal axes contain structural information about the vortex lattice. In particular, the observation of a transverse resistivity that is symmetric under reversal of the *B* field is a direct indication of spontaneous breaking of rotation symmetry by the vortex lattice. Interestingly, a *B*-symmetric transverse resistivity has been observed in experiments on vortex lattices [4,20].

We illustrate these general ideas by the rich set of vortex lattice states for frustrations 1/3 < f < 1/2. In this range, the vortex lattices are composed of a regular sequence of completely and partially filled as well as empty diagonals, see Figs. 2(a)–2(e) [13,15]. Apart from the frustration f, we characterize the states by the fraction p of partially filled diagonals as well as their filling ν . The structure of the vortex lattices is simplest for 5/14 < f < 8/21 [region II in Fig. 2(f)], where p = 1/7 and $f - p\nu = 2/7$ is the fraction of completely filled diagonals. However, our considerations below directly apply to any of the structures in Fig. 2.

The basic process governing the resistivity tensor is vortex hopping along the partially filled diagonals (Fig. 3). Stable vortex-lattice states have partially filled diagonals, which are at least half filled, $\nu > 1/2$ (see Ref. [31]). At low temperatures and for $\nu = 1/2$, the vortices organize into a regular array of alternating occupied and empty sites. Vortex motion becomes possible for $\nu > 1/2$, for which there is a finite density of occupied nearest-neighbor sites (heavy domain walls). Starting with a minimal-energy configuration of Eq. (1) with a heavy domain wall, we systematically search for adjacent saddle points (using the climbing-string method [31,32]). Subsequently, we search for new minima adjacent to the saddle point, in which the domain wall has moved by two sites. As illustrated in Fig. 3, we find that the basic process is a direct jump of the heavy domain wall along the diagonal. The saddle-point configuration has one vortex on a neighboring empty diagonal. We have not found a process with a final minimum-energy state, in which a vortex is located in an adjacent empty diagonal. From this calculation, we extract the activation barrier for a hop of a heavy domain wall. For $\nu \simeq 1/2$, we find $E_B \simeq 0.83 E_J$. For larger ν , the barrier increases slightly. For example, for f = 13/35 $(\nu = 3/5)$, one finds an energy barrier of $E_B \simeq 1.01 E_J$. The thermally activated hopping rate of a heavy domain wall along the partially filled diagonal is $\Gamma \propto \exp\{-E_R/T\}$.

Since hopping of vortices is constrained to occur along the partially filled diagonals, the resistivity tensor will be strongly anisotropic, with principal axes aligned along and perpendicular to the partially filled diagonals. In the absence of vortex hopping out of the partially filled diagonals, there is no voltage drop along the diagonals and the resistivity eigenvalue ρ_2 for currents applied along the diagonals vanishes, $\rho_2 = 0$. In contrast, current applied perpendicular to the diagonals of the vortex lattice induces vortex motion along the diagonals. This generates a voltage drop along the current direction, resulting in a nonzero resistivity eigenvalue ρ_1 .

To compute ρ_1 , we consider an applied current j_c flowing perpendicular to the diagonals of the vortex lattice. Provided that current flow is uniform, this induces potential

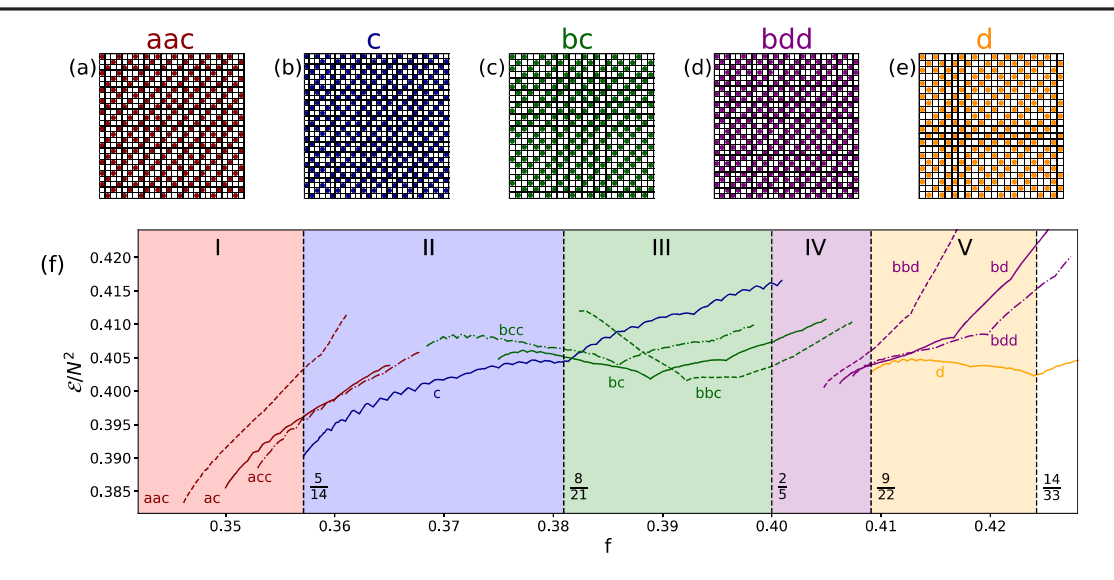


FIG. 2. (a)–(e) Vortex patterns for frustrations 1/3 < f < 1/2. The patterns are built from a set of elementary units: a = 1/3 (filled diagonal enclosed by empty diagonals on both sides), b = 2/5 (two filled diagonals enclosing an empty diagonal and enclosed by an empty diagonal on both sides), c = 5/14 (channel consisting of two 1/3 structures enclosing a partially filled diagonal), d = 9/22 (thick channel consisting of two 2/5 structures enclosing a partially filled diagonal). Additional vortices are accommodated into the partially filled diagonals, changing the frustration f by $1/N^2$. (f) Energy \mathcal{E} per lattice site of various vortex lattice structures vs f, computed by gradually filling the channels with vortices. There are five color-coded regions I–V, separated by dashed lines (with the corresponding f indicated). Results are limited to short periods between channels. This masks the transition at f = 2/5, which occurs in the limit of large periods.

drops for vortices on neighboring sites in the horizontal (\hat{x}) and vertical directions (\hat{y}) direction, which are equal to [33]

$$\Delta U = \frac{h}{2e} \frac{1}{\sqrt{2}} j_c a. \tag{4}$$

Equation (4) follows from the potential $U(\varphi) = -E_J \cos \varphi - (\hbar/2e)i_b\varphi$ of a single junction with Josephson energy E_J , phase difference φ , and bias current i_b . A vortex hopping between two neighboring plaquettes leads to a phase slip of the intermediate junction by 2π , which changes the potential by $(\hbar/2e)i_b$. Alternatively, Eq. (4) can be viewed as a manifestation of the Magnus force that the current exerts on the vortices.

For $\nu > 1/2$, there are two heavy domain walls for each additional vortex. Thus, the areal density of domain walls is equal to $2p(\nu-\frac{1}{2})(1/a^2)$. When ν is not too much larger than 1/2, the domain walls are dilute and the probability of two directly adjacent domain walls can be neglected. Accounting for the potential drop of $2\Delta U$ between initial and final state of the vortex hop in linear response, a vortex in a heavy domain wall has an effective hopping rate of $(2\Delta U/T)\Gamma$. As a result, we find an areal vortex current density of

$$j_{v} = 2p\left(\nu - \frac{1}{2}\right) \frac{\sqrt{2}}{a} \Gamma \frac{2\Delta U}{T}$$
 (5)

along the diagonals of the vortex lattice. We finally relate the vortex current density to the voltage drop in the perpendicular direction [33],

$$E = \frac{h}{2e} j_v. \tag{6}$$

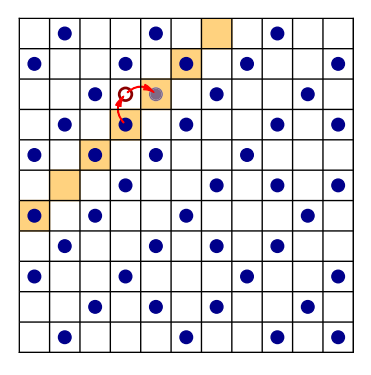


FIG. 3. Hopping process of heavy domain wall in a c structure (blue region in Fig. 2). The initial vortex configuration (dark full circles) contains a heavy domain wall (see partially filled diagonal highlighted in orange). In the adjacent saddle-point configuration, a vortex (empty circle) of the heavy domain wall hopped out of the partially filled diagonal. In the new adjacent minimum, the vortex (gray circle) returned to the partially filled diagonal, moving the heavy domain wall by two sites. We do not find minimum-energy configurations with vortices in empty diagonals.

The electric field E points in the direction perpendicular to the vortex motion and thus perpendicular to the partially filled diagonal. Combining Eqs. (4)–(6), we find the nonzero resistivity eigenvalue

$$\rho_1 = 4p \left(\nu - \frac{1}{2}\right) \left(\frac{h}{2e}\right)^2 \frac{\Gamma}{T} \tag{7}$$

in the limit of dilute domain walls.

While the partially filled diagonals order at low temperatures, numerical results indicate that these ordered arrays melt prior to the melting transition of the entire 2D vortex lattice [13]. If the interaction between vortices is sufficiently short ranged due to screening, the coupling between diagonals is weak for small p. Without coupling, the partially filled diagonals are expected to melt at any nonzero temperature by the Landau-Peierls argument. At weak coupling (small p), ordered states of the partially filled diagonals melt far below the melting temperature of the entire vortex lattice. In the intermediate regime between these melting transitions, the vortex state is akin to a smectic liquid crystal.

Well above the melting transition, we can assume that the vortex occupations become uncorrelated along the partially filled diagonals. Vortex motion along the diagonals can then be characterized by a diffusion constant $D=2a^2/\tau$ and the vortex current becomes

$$j_v = p\nu(1-\nu)\frac{1}{a^2}\frac{\sqrt{2}a}{\tau}\frac{2\Delta U}{T},\tag{8}$$

so that

$$\rho_1 = 2p\nu(1-\nu)\left(\frac{h}{2e}\right)^2 \frac{1}{T\tau}.\tag{9}$$

Unlike in the low-temperature phase, the hopping rate $1/\tau$ is no longer activated, so that the melting transition is signaled by a substantial increase in resistivity.

We now consider the resistivity tensor for currents applied along the lattice directions of the underlying square array. Rotating the resistivity tensor, we find

$$\rho = \begin{pmatrix} \rho_1/2 & \pm \rho_1/2 \\ \pm \rho_1/2 & \rho_1/2 \end{pmatrix}. \tag{10}$$

The sign of the transverse resistivities depends on the direction of the diagonal vortex structure. We also use that $\rho_H=0$ within our rate-equation theory of vortex dynamics. Because of the diagonal structure of the vortex lattice, the diagonal resistivities ρ_{xx} and ρ_{yy} are identical. The formation of the vortex lattice is still signaled by the nonzero transverse resistivity. Since vortex motion is constrained to be along the diagonal, a current applied, say, along the x axis induces equal voltage drops along the x and y

directions. Thus, ρ_{xx} and ρ_{xy}^s are equal in magnitude, which directly correlates with the diagonal structure of the vortex lattice.

Magnetic-field dependence.—There will also be substantial and characteristic variations with magnetic field. These emerge from the intricate sequence of vortex lattices for frustrations between f=1/3 and f=1/2 [13,15]. As shown in Fig. 2, the vortex lattices are built from elementary units. There are units with only completely filled and empty diagonals corresponding to the basic units of the f=1/3 and f=2/5 vortex lattices. In addition, there are units referred to as channels, which contain the partially filled diagonals (see Fig. 2 and its caption for a detailed description).

These structures were identified by Monte Carlo simulations in Refs. [13,15]. We also find such structures using a recently proposed annealing algorithm [16,31], which computes the full phase configuration. We can further confirm and extend these results using a vortex representation of the xy model [31,34,35]. Figure 2(f) compares the energy of various structures, computed numerically as a function of f by adding vortices one at a time to the partially-filled diagonals. For a given regular pattern of building blocks, we use a Metropolis algorithm to optimize the vortex arrangement along and between partially filled diagonals. Our results essentially reproduce the conclusions of Ref. [15], but indicate the existence of an additional regime originating from the previously unnoticed phase transition at f = 9/22.

The structure of the vortex lattice remains unchanged over a substantial range in magnetic field in regions II (blue) and V (yellow). Here, p remains fixed and the resistivity depends smoothly on magnetic field. In contrast, the vortex-lattice structure, and hence p as well as the resistivity tensor, depend sensitively on magnetic field in regions I (red), III (green), and IV (purple). Note that in these regions, there are more vortex-lattice states than shown in Fig. 2(f), which includes only short-sequence lattices.

Our vortex-lattice simulations use periodic boundary conditions. Boundary effects as well as disorder may lead to domains of different orientations of the vortex lattice. This reduces the anisotropy of the resistivity and hence the magnitude of ρ_{xy}^s relative to ρ_{xx} and ρ_{yy} . The reduction is a measure of the degree of domain formation of the vortex lattice.

Conclusions.—We have shown that measurements of the full resistivity tensor are a powerful tool to identify and probe the rich set of symmetry-breaking vortex-lattice states as a function of magnetic field, providing both structural and dynamical information. This includes the liquid-crystalline vortex states above the melting transition of the partially filled diagonals, which have the remarkable property of being resistive in one direction and superconducting in the other. We note that the signatures of

symmetry-breaking ground states in the resistivity are expected to persist beyond the assumptions made in Eq. (1). Our general approach also carries over to other (nematic) electronic states which break an underlying rotational symmetry (for a very recent discussion, see Ref. [36]).

We have focused on vortex configurations aligned along the diagonal, which have particularly transparent vortex dynamics. In principle, one expects anisotropic resistivity tensors also for other symmetry-breaking vortex-lattice states. This includes states such as the f=1/5 state [see Fig. 1(c)], whose principal axes are rotated by other angles, so that ρ_{xx} and ρ_{yy} are different from each other. In this case, measurements of the full resistivity tensor may also contribute to elucidating the underlying vortex dynamics.

Our discussion neglected capacitive effects and was limited to classical modeling. While our qualitative conclusions are expected to persist, it is an interesting question for future work to relax these assumptions and account for quantum fluctuations, which may, e.g., induce a nonzero Hall resistivity ρ_H .

We thank C. M. Marcus for discussions stimulating the present work. Financial support was provided by Deutsche Forschungsgemeinschaft through CRC 183, the Einstein Research Unit on Quantum Devices, the Danish National Research Foundation, the Danish Council for Independent Research | Natural Sciences, the European Research Council (ERC) under the European Union's Horizon 2020 research and innovation program under Grant 856526, National Agreement No. the Foundation through Grant No. DMR-2002275, and the Office of Naval Research (ONR) under Award No. N00014-22-1-2764. L. I. G. thanks Freie Universität Berlin for hosting him as a CRC 183 Mercator fellow.

- J. C. Ciria and C. Giovannella, J. Phys. Condens. Matter 10, 1453 (1998).
- [2] R. Fazio and H. S. J. van der Zant, Phys. Rep. **355**, 235 (2001).
- [3] B. Pannetier, J. Chaussy, R. Rammal, and J. C. Villegier, Phys. Rev. Lett. 53, 1845 (1984).
- [4] B. J. van Wees, H. S. J. van der Zant, and J. E. Mooij, Phys. Rev. B 35, 7291 (1987).
- [5] L. N. Vu, M. S. Wistrom, and D. J. Van Harlingen, Appl. Phys. Lett. 63, 1693 (1993).
- [6] H. D. Hallen, R. Seshadri, A. M. Chang, R. E. Miller, L. N. Pfeiffer, K. W. West, C. A. Murray, and H. F. Hess, Phys. Rev. Lett. 71, 3007 (1993).
- [7] S. Teitel and C. Jayaprakash, Phys. Rev. Lett. **51**, 1999 (1983).

- [8] T. C. Halsey, Phys. Rev. B 31, 5728 (1985).
- [9] M. R. Kolahchi and J. P. Straley, Phys. Rev. B 43, 7651 (1991).
- [10] A. Vallat and H. Beck, Phys. Rev. Lett. 68, 3096 (1992).
- [11] J. P. Straley and G. M. Barnett, Phys. Rev. B 48, 3309 (1993).
- [12] M. Franz and S. Teitel, Phys. Rev. B 51, 6551 (1995).
- [13] P. Gupta, S. Teitel, and M. J. P. Gingras, Phys. Rev. Lett. 80, 105 (1998).
- [14] C. Denniston and C. Tang, Phys. Rev. B 60, 3163 (1999).
- [15] S. J. Lee, J.-R. Lee, and B. Kim, Phys. Rev. Lett. **88**, 025701 (2001).
- [16] M. Lankhorst, A. Brinkman, H. Hilgenkamp, N. Poccia, and A. Golubov, Condens. Matter 3, 19 (2018).
- [17] F. Falo, A. R. Bishop, and P. S. Lomdahl, Phys. Rev. B 41, 10983 (1990).
- [18] A. van Otterlo, K.-H. Wagenblast, R. Fazio, and G. Schön, Phys. Rev. B 48, 3316 (1993).
- [19] P. Martinoli, R. Theron, J.-B. Simond, R. Meyer, Y. Jaccard, and C. Leemann, Phys. Scr. 1993, 176 (1993).
- [20] C. M. Marcus (private communication).
- [21] L. Balents and D. R. Nelson, Phys. Rev. B 52, 12951 (1995).
- [22] J. Shabani, M. Kjaergaard, H. J. Suominen, Y. Kim, F. Nichele, K. Pakrouski, T. Stankevic, R. M. Lutchyn, P. Krogstrup, R. Feidenhans'l, S. Kraemer, C. Nayak, M. Troyer, C. M. Marcus, and C. J. Palmstrøm, Phys. Rev. B 93, 155402 (2016).
- [23] C. G. L. Bøttcher, F. Nichele, M. Kjaergaard, H. J. Suominen, J. Shabani, C. J. Palmstrøm, and C. M. Marcus, Nat. Phys. 14, 1138 (2018).
- [24] C. G. L. Bøttcher, F. Nichele, J. Shabani, C. J. Palmstrøm, and C. M. Marcus, arXiv:2210.00318.
- [25] C. G. L. Bøttcher, F. Nichele, J. Shabani, C. J. Palmstrøm, and C. M. Marcus, arXiv:2212.08651.
- [26] K. Nakajima and Y. Sawada, J. Appl. Phys. **52**, 5732 (1981).
- [27] A. Majhofer, T. Wolf, and W. Dieterich, Phys. Rev. B 44, 9634 (1991).
- [28] A. Petraglia, G. Filatrella, and G. Rotoli, Phys. Rev. B 53, 2732 (1996).
- [29] J. R. Phillips, H. S. J. van der Zant, J. White, and T. P. Orlando, Phys. Rev. B 47, 5219 (1993).
- [30] J. R. Phillips, H. S. J. van der Zant, J. White, and T. P. Orlando, Phys. Rev. B 50, 9387 (1994).
- [31] See Supplemental Material at http://link.aps.org/supplemental/10.1103/PhysRevLett.131.206001 for details on the numerical calculations and additional discussion of Fig. 2(f).
- [32] W. Ren and E. Vanden-Eijnden, J. Chem. Phys. **138**, 134105
- [33] B. I. Halperin and D. R. Nelson, J. Low Temp. Phys. **36**, 599 (1979).
- [34] J. V. José, L. P. Kadanoff, S. Kirkpatrick, and D. R. Nelson, Phys. Rev. B **16**, 1217 (1977).
- [35] S. Teitel, in 40 Years of Berezinskii–Kosterlitz–Thouless Theory (World Scientific, Singapore, 2013), pp. 201–235.
- [36] J. D. Sau and S. Tewari, arXiv:2306.06840.